Received: 30 April 2021 | Accepted: 11 May 2021

DOI: 10.1002/ctpp.202100081

ORIGINAL ARTICLE

Contributions to Plasma Physics

Formation of droplets in weightless complex plasmas

Eshita Joshi[1] | **Sergey Khrapak**[2] | **Christina Knapek**[1] | **Peter Huber**[1] | **Daniel Mohr**[1] | **Mierk Schwabe**[1]

[1]Institut für Materialphysik im Weltraum, Deutsches Zentrum für Luft- und Raumfahrt, Weßling, Germany

[2]Joint Institute for High Temperatures, Russian Academy of Sciences, Moscow, Russia

Correspondence
Eshita Joshi, Institut für Materialphysik im Weltraum, Deutsches Zentrum für Luft- und Raumfahrt, 82234 Weßling, Germany.
Email: eshita.joshi@dlr.de

Funding information
Bayerisches Staatsministerium für Wirtschaft und Medien, Energie und Technologie; DLR/BMWi FKZ, Grant/Award Number: 50WM1441; Ministry of Science and Higher Education of the Russian Federation, Grant/Award Number: 075-00892-20-01; Nachwuchsgruppenprogram DLR-Geschäftsbereich Raumfahrtforschung und -technologie; Deutsches Zentrum für Luft- und Raumfahrt

Abstract

Microparticles immersed in a low-temperature plasma acquire strong negative charges and thus repel each other. Nevertheless, effective attraction between the microparticles in such a complex plasma can occur due to the interplay between the fluxes of plasma ions and the microparticles. Here, we report the observation of droplets formed in a complex plasma during a parabolic flight, and explain their formation in terms of the ion drag force that sustains the droplet. We have found a good agreement between the experimentally determined droplet size and its theoretical estimate using the ion drag force mechanism. Lower values of the electron temperature result in better agreement, as is consistent with the pulsed mechanism of discharge used experimentally.

KEYWORDS

complex plasma, droplets, dust structures, dusty plasma, ion drag force

1 | INTRODUCTION

In recent years, the assembly and control of structures such as clusters and crystals in low-temperature plasma reactors have gained an increasing popularity.[1–3] Understanding their formation and the mechanisms controlling their behaviour is important for the development of, for example, nanomaterials.[4] Under the influence of an external confinement, the formation of microparticle (dust) clusters or Yukawa balls consisting from only a few up to thousands of dust particles has been observed.[5] In these systems, the microparticles attain high negative charges due to the fluxes of plasma ions and electrons onto their surfaces.[6] The microparticles interact with each other via a screened Coulomb/Yukawa potential and attain inter-particle distances of the order of 100 μm, which is large compared to their sizes of a few μm. Thus, the microparticle systems are transparent and can be imaged using simple techniques. Recording laser light scattered by the microparticles makes it possible to trace their motion from frame to frame and perform studies on the kinetic level.

Since all microparticles are charged negatively, some external force is required to confine them—this is usually achieved with an electric field, for example, by using that the surfaces of a glass box placed on the bottom electrode of the plasma reactor automatically charge up negatively with respect to the plasma, or simply by using the ambipolar electric field of the plasma.

However, the condensation of microparticles into clusters, sometimes called "boundary-free" clusters, without an increased external confinement has also been observed in cryogenic plasmas,[7,8] direct current (DC),[9] and radio-frequency (RF) plasmas.[10–12] The formation of these clusters was predicted to take place for dense microparticle clouds due to the mutual shadowing of plasma flows onto these particles,[13–16] or due to the fact that newly created ions in the space between microparticles will lead to an effective positive space charge with overlapped ion clouds as well as reduced microparticle charge and electron number density in these dense clouds.[4,17] A self-confinement of pairs of microparticles can also occur due to the non-reciprocity of the inter-particle interaction.[18]

Another mechanism that could cause an effective attraction between the negatively charged microparticles is the ion drag force, which is the force induced by ions streaming past the microparticles. It is well known that the ion drag force leads to an effective attraction at intermediate distances of microparticles to a large object in the plasma such as a probe or a sphere.[19–26] In this work, we will first discuss new observations of droplet formation in a complex plasma under microgravity conditions, and then discuss these observations in the framework of ion drag theories.

2 | EXPERIMENTAL OBSERVATIONS

2.1 | On the ground with PK-3 Plus chamber

Previously, self-confined droplets have been observed in the PK-3 Plus chamber on ground when gravity was compensated by thermophoresis.[10,11] The PK-3 Plus chamber consists of a capacitively coupled RF plasma chamber with an electrode separation of 3 cm.[27] One version of this setup was located on board the International Space Station ISS[28,29] and another version in the ground laboratory.[30] Droplet formation was only observed on ground when the bottom electrode was heated to produce a temperature gradient that was able to compensate for the force of gravity on the microparticles. This was probably not seen in microgravity on the space station because a collection of particles never moved into the void. On ground, this temperature gradient led to a convection of the background gas,[31,32] which accelerated microparticles from the region below the particle-free central void into the void, where they often condensed into droplets. Figure 1a shows such a microparticle droplet in the PK-3 Plus chamber with 7.2 μm sized melamine-formaldehyde particles.

2.2 | Parabolic flight with Zyflex chamber

Recently, we observed that droplets formed in the Zyflex chamber during the weightless phase of a parabolic flight. This can be seen in Figure 1b. The Zyflex chamber is a versatile RF plasma chamber that forms the basis of the COMPACT laboratory destined to be the next complex plasma research facility on board the ISS.[33,34] It combines several advances compared to the PK-3 Plus chamber; most notably, its electrodes are larger with an outer electrode diameter of 120 mm

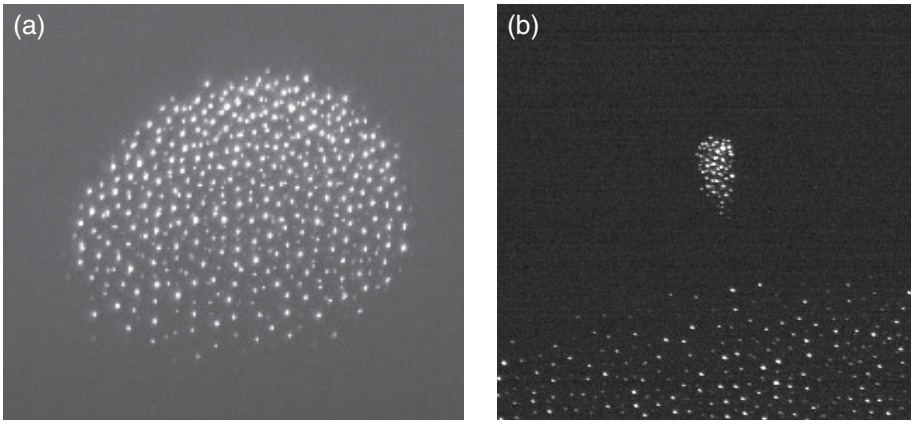

FIGURE 1 (a) Droplet in the PK-3 Plus chamber when gravity was compensated for by thermophoresis (field of view: $4 \times 4\,\mathrm{mm}^2$, 7.2 μm particles, $\Delta T = 63$ K, argon gas at 18 Pa, from ref. [11]), and (b) in the Zyflex chamber under microgravity conditions (field of view: $11 \times 11\,\mathrm{mm}^2$, in the bottom the main particle cloud is visible, 4.4 μm particles, argon gas at 5 Pa)

compared with the 60 mm of the PK-3 Plus chamber, and the electrode distance can be varied between 25 and 75 mm. Two opposing electrodes (top and bottom) are mounted in the chamber, with each electrode consisting of two electrically isolated segments: one central disk encircled by a ring electrode. Each segment is driven independently by its own RF source for plasma generation.

The experiment was performed with an electrode distance of 75 mm and a neutral gas pressure of 5 Pa (Argon). The plasma was generated by RF signals on the electrodes, with a peak-to-peak voltage of 60 V on all electrode segments. Further, the RF signals were pulsed in a continuously repeating diagonal pattern: the top ring and bottom center segments were switched on for 200 μs, then switched off, while the top center and bottom ring segments were simultaneously powered for the next 200 μs. The pulsing was used to lower the electron temperature on a time average,[35] but did not directly affect the microparticles due to the short switching time scale.

The plasma parameters obtained from particle-in-cell (PIC) simulations (using the xoopic code version 2.70,[36]) show that typical electron densities in the Zyflex chamber driven in continuous mode are in the range $1.2 - 2.4 \times 10^{14} \mathrm{m}^{-3}$, and electron temperatures are between 2.3−2.9 eV for 5 Pa and 75 mm electron distance. The simulations were performed for a slightly lower peak-to-peak voltage of 40 V.[34]

Though no simulations are available for the pulsed discharge, the literature indicates that the plasma density is of the same order of magnitude for pulsed and continuous plasma, while the electron temperature usually decreases rapidly during a pulse period. Therefore, the time average of T_e should be considerably lower than the continuous plasma case.[37]

Spherical melamine-formaldehyde particles with 4.4 μm diameter were injected into the plasma at the beginning of the weightless phase. Particles were illuminated by a thin laser sheet, yielding a view of a quasi 2D cross section through the 3D system. The reflected light was then recorded by video cameras. Figure 1b shows a droplet that formed during the parabola. The void forms in the center of the discharge[38–41] as the particles move outwards since in that region the drag force of ions streaming towards the chamber walls is larger than the electric force that confined the microparticles. The droplets condensed out of a group of microparticles that were still present in the central, typically particle-free void area after the initial particle injection. The density inside the droplet (within the illuminated plane) was estimated to be $41 \pm 5\,\mathrm{mm}^{-2}$, corresponding to a "2D inter-particle distance" of 177 ± 11 μm.

The droplet moved inside the void relative to the microparticles in the main microparticle cloud. This motion is shown in Figure 2, which tracks the droplet position using colour to mark the passage of time.

3 | THEORETICAL CONSIDERATIONS

Here, we consider a possible mechanism for the formation of a droplet in terms of the ion drag force. A notable detail about droplet formation is that it always occurred in the void region, which is a quasineutral, typically particle-free region characterized by slow-moving subthermal ions. In previous ground-based experiments, which compensated gravity by thermophoresis, droplet formation was observed when the convection currents of the background gas lifted particles from the main dust cloud into the particle-free central void.[10,11] Similarly, in the parabolic flight experiment, the particles in the void condensed into droplets. Our hypothesis for the mechanism behind this particle condensation is the following:

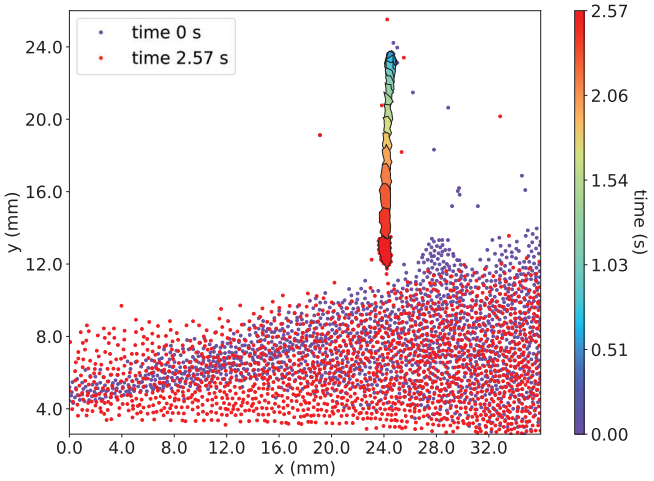

FIGURE 2 Superposition of particle positions colour-coded to indicate time. In the bottom, only the positions of particles inside a part of the main particle cloud in the beginning (blue) and end (red) of the time sequence are shown. Above these, a droplet indicated with filled contours is seen to move from the top towards the bottom

once there is a collection of negatively charged particles in the void, they start attracting the ions around them. The accelerating ions exert a pressure on the dust particles, which is higher on the "outside" than it is between the particles. This is true as long as the particles are not far enough apart to be effectively isolated. It should be noted here that we are neglecting the effect of ion shadowing and charge cannibalism for the purpose of testing the above hypothesis.

The pressure anisotropy due to the ion flow causes the particles to move closer together. As the inter-particle distance starts decreasing, the electrostatic repulsion between the particles starts increasing. The particles continue to move closer together until the electrostatic repulsion increases to match the pressure from the ion flow. Once the electrostatic repulsive force is in balance with the ion drag force, a stable droplet is formed. We can test whether the equilibrium reached by the two forces, and hence the droplet radius, is stable or unstable by the following thought experiment. Should the particles continue moving closer together to form a smaller droplet, the repulsion would increase to be higher than the inward pressure. This would result in a counteracting increase in droplet radius, returning the droplet to its equilibrium size. On the other hand, if the particles move away from each other to form a larger droplet, the electrostatic repulsion reduces to be lower than the pressure associated with the ion drag force. This, instead, causes a counteracting reduction in droplet radius. Thus, we arrive at a stable configuration of particles that should retain the droplet shape as long as the plasma parameters remain the same.

We can test this hypothesis by balancing the forces on a particle at the droplet boundary and finding how the radius of the droplet depends on plasma parameters. We then check whether the obtained result is consistent with the experimental observations.

3.1 | Important length scales

It is useful to first summarize the main length scales for the problem at hand. The smallest is the particle radius, which is $a = 2.2$ μm. The inter-particle distance within the droplet is of the order $\Delta \sim 100$ μm from experimental observations. For simplicity, we assume that the particle density inside the droplet is homogeneous. The electron Debye radius can be estimated using

$$\lambda_e = \sqrt{\frac{T_e}{4\pi e^2 n_e}}, \tag{1}$$

which gives us $\lambda_e \sim 500$ μm, where T_e is the electron temperature in energy units and n_e is the electron density (we have assumed $n_e \sim 2 \times 10^8$ cm^{-3} based on the results from the PIC simulation, and $T_e \sim 1$ eV since the electron temperature in the pulsed discharge is expected to be lower than that of a continuous discharge). The radius of droplets observed experimentally is in the millimetre range, $R \sim 1$ mm. The number of particles inside a droplet can be estimated by assuming cuboidal packing from

$$N = \frac{4\pi}{3}\left(\frac{R}{\Delta}\right)^3, \tag{2}$$

which would result in few thousands per millimetre size droplet. We will assume $N = 1{,}000$ for the rough estimates presented below.

3.2 | The ion drag force

A droplet formed in the bulk plasma effectively acts as a body (e.g., probe) immersed in a plasma. The electric potential inside the droplet is negative with respect to the surrounding plasma and the fluxes of electrons and ions are directed towards its surface (these electrons and ions are then collected by particles inside the droplet). It is legitimate to assume that a sheath is formed between the droplet and the plasma, and that this sheath is thin in the first approximation (since the electron Debye radius is smaller than the droplet size). Ions enter the sheath with a near-sonic velocity, $v_i \sim \sqrt{T_e/m_i}$, where m_i is the ion mass. This may serve as a rough estimate of the ion velocity near the droplet surface. For highly super-thermal ion velocities, the force associated with the momentum transfer from the drifting ions—the ion drag

force—can be evaluated from refs. [6,42–44].

$$F_{id} = n_i m_i v_i^2 \sigma, \tag{3}$$

where σ is the momentum transfer cross section and n_i denotes the ion number density. Two mechanisms contribute as follows: direct collection and scattering on the charged particle electric potential. The collection cross section is just the geometrical one

$$\sigma_{\text{coll}} = \pi a^2.$$

The scattering cross section is the conventional Coulomb cross section.[40,45]

$$\sigma_{\text{s}} = \frac{4\pi Q^2 e^2}{m_i^2 v_i^4} \ln \Lambda,$$

where Q is the particle charge and $\ln\Lambda$ is the Coulomb logarithm. For near-sonic ions we get

$$\sigma_{\text{s}}/\sigma_{\text{coll}} \simeq 4 \left(\frac{Q^2 e^2}{a^2 T_e^2} \right) \ln \Lambda.$$

Since high ion flow velocities make ineffective the ion-neutral collisional enhancement of the ion flux to the particle,[46] and since a relatively low pressure was used, we can expect that the reduced particle charge is above unity, $z = |Q|\, e/aT_e > 1$. Additionally, for highly super-thermal ion flows, plasma screening is mostly associated with electrons, while the distance of the closest approach between a near-sonic ion and a particle is of the order of the particle radius ($|Q|\, e/m_i v_i^2 \simeq |Q|\, e/T_e \sim a$). Thus, we get for the Coulomb logarithm $\ln \Lambda \simeq \ln(\lambda_e/a) \simeq 5$ in the parameter regime investigated. So, we have to expect that the ion drag force is mostly associated with Coulomb scattering and the following estimate applies

$$F_{id} \simeq 4\pi n_i \left(\frac{Q^2 e^2}{T_e} \right) \ln \Lambda. \tag{4}$$

Flowing electrons also transfer momentum to the particles. However, their effect is negligible in the considered situation because their flux is the same as that of the ions, but their mass and hence momentum are much smaller.[47]

3.3 | Force balance

The ion drag force, pushing the particles in the droplet closer to each other, should be balanced by an outward electric force due to inter-particle repulsion. Assuming that the electric charge inside the droplet is dominated by the particle component, the electric field at the droplet boundary, E, can be simply estimated as follows:

$$E \simeq \frac{QN}{R^2}. \tag{5}$$

The electric force acting on a particle on the surface can be estimated as follows:

$$F_e \simeq QE \simeq \frac{Q^2 N}{R^2}. \tag{6}$$

Equating Equations (4) and (6), and using the quasineutrality condition of $n_i = n_e$ along with the definition of λ_e from Equation (1), we get

$$R \simeq \lambda_e \left(\frac{N}{\ln \Lambda} \right)^{1/2}. \tag{7}$$

For the parameters specified above this results in $R \simeq 7$ mm, which is an upper estimate of the droplet size and exceeds the size observed experimentally. This is because we neglected the partial compensation of the electric charge inside the cloud, provided by the electrons and ions. If the latter is taken into account, the force that a particle located near the droplet surface experiences is just repulsion from nearest neighbours located deeper inside the droplet. Since $\Delta < \lambda_e$, we can neglect screening in the first approximation (we remind the reader that screening is mostly due to electrons for near-sonic ions). Then, omitting geometrical numerical factors of order unity, the repulsive force can just be estimated as the Coulomb force at the mean inter-particle separation,

$$F_e \simeq \frac{Q^2}{\Delta^2}. \tag{8}$$

Equating Equations (4) and (8) and taking into account the relation between the mean inter-particle separation and the droplet radius from Equation (2), we now get

$$R \simeq \lambda_e \left(\frac{3N}{4\pi}\right)^{1/3} (\ln \Lambda)^{-1/2}. \tag{9}$$

This estimate can be considered as a lower estimate of the droplet size. Depending on the assumptions and parameters specified above, it yields $R \simeq 1.4$ mm for the characteristic parameters specified earlier, which is comparable to experimental observations. Thus, the simple mechanism proposed seems to provide an explanation of the droplet formation and is able to approximately predict its size.

4 | RESULTS AND DISCUSSION

We test the model presented above by studying how the radius of the droplet varies with experimental parameters, and by checking whether using the experimentally determined parameters in the model results in a droplet size similar to what was measured.

The number of particles in the droplet is between a few hundred to a few thousand in the various experiments. In the parabolic flight experiment, the number is estimated to be between 100 and 700, whereas in the ground-based experiments, the estimate is around 3000–5000. The dependence of the radius on the number of particles is shown in Figure 3, where it can be seen that the radius increases rapidly with increasing N for the first few hundreds of particles. The increase starts slowing down as N approaches a few thousand. This trend can also be seen in the experiments, where the ground-based droplet shown in Figure 1a has an order of magnitude more particles than the parabolic flight droplet shown in Figure 1b, and yet is only about 1 mm larger.

As mentioned in section 2.2, the time averaged electron temperature for the experiment with the pulsed discharge could be considerably lower than the temperature in the continuous discharge. Figure 3 also shows how decreasing T_e decreases the estimated droplet radius for a fixed number of particles. The size of the droplet observed in the 2D laser sheet during the parabolic flight experiment is estimated to be 0.9 mm × 1.4 mm. Using $N = 500$ as the estimated number of particles in the observed droplet and $a = 2.2$ μm as the particle radius, the lower estimate for the droplet radius predicted

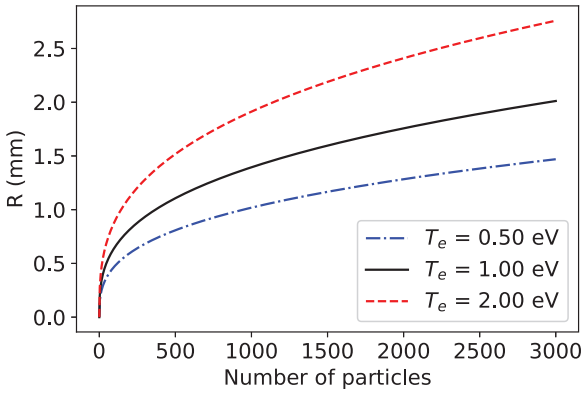

FIGURE 3 Dependence of droplet radius on the number of particles, N, in the droplet for various values of electron temperatures, T_e according to Equation (9). Lower values of T_e for a fixed N result in better agreement with experimental data. Note that the assumption that the Debye radius is smaller than the droplet size does not hold true for $R < 0.5$ mm

by Equation (9) with $T_e = 0.5$ eV is $\simeq$0.8 mm, with $T_e = 1.0$ eV is $\simeq$1.1 mm, and with $T_e = 2.0$ eV is $\simeq$1.5 mm. As expected, the model agrees with the experimental observations better for values of T_e significantly lower than the approximate 2.0 eV predicted by the continuous discharge PIC simulation.

5 | CONCLUSION

We have reported the observation of microparticles detaching themselves from the main particle cloud and condensing into droplets in the dust-free void during a parabolic flight. We have suggested that the formation of these droplets in weightless complex plasmas can be explained by the ion drag force mechanism and studied the effect of plasma parameters on the size of these droplets. The experimentally observed size of the droplet was estimated to be 0.9 mm $\times$ 1.4 mm in the illuminated plane, and the theoretical lower estimate for the droplet radius given the same parameters was predicted to be $\simeq$1.1 mm and $\simeq$0.8 mm using electron temperatures of 1.0 eV and 0.5 eV, respectively. Both of these temperatures are considerably smaller than those predicted by the continuous discharge PIC simulation. We have thus found that there is good agreement between the model and experiment for low values of T_e. This is in agreement with our expectation of reduced electron temperatures in the experiment due to the pulsing of the discharge.

In the future, a more detailed study of the experimental parameters during pulsing is planned, and thus a more precise comparison with the model will be possible. Our model assumed that the droplets are perfect spheres, however, anisotropies in droplet radius have been observed. We believe that the model is still applicable to elongated droplets, but perhaps a future study can either test this or incorporate radius anisotropies into the model. Our model did not take into account the effects of charge cannibalism or try to estimate the particle charge. Since the model doesn't depend on the absolute magnitude of the particle charge, a future study might be better suited to investigate the extent to which charge cannibalism affects the stability of the droplet.

ACKNOWLEDGMENTS

We acknowledge funding of this work in the framework of the Nachwuchsgruppenprogram im DLR-Geschäftsbereich Raumfahrtforschung und -technologie. C. A. Knapek, P. Huber and D. P. Mohr were funded by DLR/BMWi FKZ (50WM1441) and the Bavarian Ministry of Economic Affairs and Media, Energy and Technology (StMWi). Theoretical work on plasma-particle interactions in dusty plasmas was partly supported by the Ministry of Science and Higher Education of the Russian Federation (State Assignment No. 075-00892-20-01). We would like to thank Philip Born for careful reading of the manuscript, and Hubertus Thomas for his support. Open Access funding enabled and organized by Projekt DEAL.

DATA AVAILABILITY STATEMENT

Data sharing is not applicable as all new data are available in the paper itself.

ORCID

Eshita Joshi https://orcid.org/0000-0001-8557-1141
Sergey Khrapak https://orcid.org/0000-0002-3393-6767
Christina Knapek https://orcid.org/0000-0001-7105-627X
Peter Huber https://orcid.org/0000-0002-1426-6104
Daniel Mohr https://orcid.org/0000-0002-9382-6586
Mierk Schwabe https://orcid.org/0000-0001-6565-5890

REFERENCES

[1] S. V. Vladimirov, A. A. Samarian, *Plasma Phys. Control. Fusion* **2007**, *49*, B95.
[2] H. Thomsen, P. Ludwig, M. Bonitz, J. Schablinski, D. Block, A. Schella, A. Melzer, *J. Phys. D Appl. Phys.* **2014**, *47*, 383001.
[3] I. Adamovich, S. D. Baalrud, A. Bogaerts, P. J. Bruggeman, M. Cappelli, V. Colombo, U. Czarnetzki, U. Ebert, J. G. Eden, P. Favia, D. B. Graves, S. Hamaguchi, G. Hieftje, M. Hori, I. D. Kaganovich, U. Kortshagen, M. J. Kushner, N. J. Mason, S. Mazouffre, S. M. Thagard, H. R. Metelmann, A. Mizuno, E. Moreau, A. B. Murphy, B. A. Niemira, G. S. Oehrlein, Z. L. Petrovic, L. C. Pitchford, Y. K. Pu, S. Rauf, O. Sakai, S. Samukawa, S. Starikovskaia, J. Tennyson, K. Terashima, M. M. Turner, M. C. M. van de Sanden, A. Vardelle, *J. Phys. D Appl. Phys.* **2017**, *50*, 323001.
[4] G. V. Miloshevsky, A. Hassanein, *Phys. Rev. E* **2012**, *85*, 056405.
[5] A. Melzer, B. Buttenschön, T. Miksch, M. Passvogel, D. Block, O. Arp, A. Piel, *Plasma Phys. Control. Fusion* **2010**, *52*, 124028.

[6] A. Melzer, Physics of Dusty Plasmas, Springer, Cham, Switzerland, **2019**.
[7] E. Asinovskii, A. Kirillin, V. Markovets, *Phys. Lett. A* **2006**, *350*, 126.
[8] S. N. Antipov, M. M. Vasiliev, O. F. Petrov, *Contrib. Plasma Physics* **2012**, *52*, 203.
[9] A. D. Usachev, A. Zobnin, O. F. Petrov, V. E. Fortov, B. M. Annaratone, M. H. Thoma, H. Höfner, M. Kretschmer, M. Fink, G. E. Morfill, *Phys. Rev. Lett.* **2009**, *102*, 045001.
[10] M. Schwabe, M. Rubin-Zuzic, S. Zhdanov, A. V. Ivlev, H. M. Thomas, G. E. Morfill, *Phys. Rev. Lett.* **2009**, *102*, 255005.
[11] M. Schwabe, Ph.D. thesis, Ludwig-Maximilians-Universität **2009**.
[12] B. M. Annaratone, T. Antonova, C. Arnas, P. Bandyopadhyay, M. Chaudhuri, C. R. Du, Y. Elskens, A. V. Ivlev, G. E. Morfill, V. Nosenko, K. R. Sütterlin, M. Schwabe, H. M. Thomas, *Plasma Sources Sci. Technol.* **2010**, *19*, 065026.
[13] V. N. Tsytovich, *Comm. Plasma Phys. Control. Fusion* **1994**, *15*, 349.
[14] A. M. Ignatov, *Plasma Phys. Rep.* **1996**, *22*, 585.
[15] S. A. Khrapak, G. E. Morfill, *Phys. Plasmas* **2008**, *15*, 084502-1.
[16] M. Lampe, G. Joyce, *Phys. Plasmas* **2015**, *22*, 023704.
[17] V. N. Tsytovich, G. E. Morfill, *Plasma Phys. Rep.* **2002**, *28*, 171.
[18] I. I. Lisina, E. A. Lisin, O. S. Vaulina, O. F. Petrov, *Physical Review E* **2017**, *95*(1), 013202.
[19] D. A. Law, W. H. Steel, B. M. Annaratone, J. E. Allen, *Phys. Rev. Lett.* **1998**, *80*, 4189.
[20] C. O. Thompson, N. D'Angelo, R. L. Merlino, *Phys. Plasmas* **1999**, *6*, 1421.
[21] D. Samsonov, A. V. Ivlev, G. E. Morfill, J. Goree, *Phys. Rev. E* **2001**, *63*, 025401(R).
[22] E. Thomas Jr., K. Avinash, R. L. Merlino, *Phys. Plasmas* **2004**, *11*, 1770.
[23] M. Klindworth, O. Arp, A. Piel, *Rev. Sci. Instrum.* **2007**, *78*, 033502.
[24] B. J. Harris, L. S. Matthews, T. W. Hyde, *Phys. Rev. E* **2015**, *91*, 063105.
[25] M. Schwabe, S. K. Zhdanov, T. Hagl, P. Huber, A. M. Lipaev, V. I. Molotkov, V. Naumkin, M. Rubin-Zuzic, P. V. Vinogradov, E. Zaehringer, V. E. Fortov, H. M. Thomas, *New J. Phys.* **2017**, *19*, 103019.
[26] S. Khrapak, P. Huber, H. Thomas, V. Naumkin, V. Molotkov, A. Lipaev, *Physical Review E* **2019**, *99*, 053210.
[27] H. M. Thomas, G. E. Morfill, V. E. Fortov, A. V. Ivlev, V. I. Molotkov, A. M. Lipaev, T. Hagl, H. Rothermel, S. A. Khrapak, R. K. Sütterlin, M. Rubin-Zuzic, O. F. Petrov, V. I. Tokarev, S. K. Krikalev, *New J. Phys.* **2008**, *10*, 033036.
[28] M. Schwabe, C. R. Du, P. Huber, A. M. Lipaev, V. I. Molotkov, V. N. Naumkin, S. K. Zhdanov, D. I. Zhukhovitskii, V. E. Fortov, H. M. Thomas, *Microgravity Sci. Technol.* **2018**, *30*(5), 581.
[29] H. M. Thomas, M. Schwabe, M. Pustylnik, C. A. Knapek, V. I. Molotkov, A. M. Lipaev, O. F. Petrov, V. E. Fortov, S. Khrapak, *Plasma Phys. Control. Fusion* **2019**, *61*, 014004.
[30] H. Rothermel, T. Hagl, G. E. Morfill, M. H. Thoma, H. M. Thomas, *Phys. Rev. Lett.* **2002**, *89*, 175001.
[31] S. Mitic, R. Sütterlin, A. V. Ivlev, H. Höfner, M. H. Thoma, S. Zhdanov, G. E. Morfill, *Phys. Rev. Lett.* **2008**, *101*, 235001.
[32] M. Schwabe, L. J. Hou, S. Zhdanov, A. V. Ivlev, H. M. Thomas, G. E. Morfill, *New J. Phys.* **2011**, *13*, 083034.
[33] C. A. Knapek, P. Huber, D. P. Mohr, E. Zaehringer, V. I. Molotkov, A. M. Lipaev, V. Naumkin, U. Konopka, H. M. Thomas, V. E. Fortov, *AIP Conf. Proc.* **2018**, *1925*, 020004.
[34] C. Knapek, U. Konopka, D. P. Mohr, P. Huber, A. M. Lipaev, H. M. Thomas, unpublished.
[35] J. P. Booth, G. Cunge, N. Sadeghi, R. W. Boswell, *J. Appl. Phys.* **1997**, *82*(2), 552.
[36] J. P. Verboncoeur, A. B. Langdon, N. T. Gladd, *Comput. Phys. Commun.* **1995**, *87*, 199.
[37] M. Lieberman, A. Lichtenberg, Principles of Plasma Discharges and Materials Processing, Wiley, Hoboken, NJ, **2005**.
[38] G. E. Morfill, H. M. Thomas, U. Konopka, H. Rothermel, M. Zuzic, A. Ivlev, J. Goree, *Phys. Rev. Lett.* **1999**, *83*, 1598.
[39] J. Goree, G. E. Morfill, V. N. Tsytovich, S. V. Vladimirov, *Phys. Rev. E* **1999**, *59*, 7055.
[40] S. A. Khrapak, A. V. Ivlev, G. E. Morfill, H. M. Thomas, *Phys. Rev. E* **2002**, *66*, 046414.
[41] A. M. Lipaev, S. A. Khrapak, V. I. Molotkov, G. E. Morfill, V. E. Fortov, A. V. Ivlev, H. M. Thomas, A. G. Khrapak, V. N. Naumkin, A. I. Ivanov, S. E. Tretschev, G. I. Padalka, *Phys. Rev. Lett.* **2007**, *98*, 265006.
[42] M. S. Barnes, J. H. Keller, J. C. Forster, J. A. O'Neill, D. K. Coultas, *Phys. Rev. Lett.* **1992**, *68*(3), 313.
[43] M. Hirt, D. Block, A. Piel, *Phys. Plasmas* **2004**, *11*, 5690.
[44] S. A. Khrapak, A. V. Ivlev, S. K. Zhdanov, G. E. Morfill, *Phys. Plasmas* **2005**, *12*, 042308.
[45] E. Lifshitz, L. P. Pitaevskii, Physical Kinetics, Elsevier Science, Stanford, CA **1995**.
[46] S. A. Khrapak, M. H. Thoma, M. Chaudhuri, G. E. Morfill, A. V. Zobnin, A. D. Usachev, O. F. Petrov, V. E. Fortov, *Phys. Rev. E* **2013**, *87*(6), 063109.
[47] S. A. Khrapak, G. E. Morfill, *Phys. Rev. E* **2004**, *69*, 066411.

How to cite this article: E. Joshi, S. Khrapak, C. Knapek, P. Huber, D. Mohr, M. Schwabe, *Contributions to Plasma Physics* **2021**, e202100081. https://doi.org/10.1002/ctpp.202100081